Comparison of Adaptive Control Architectures for Flutter Suppression

A Comparison of Adaptive Control Architectures for Flutter Suppression

M. Cassaro[1] and M. Battipede[2]
Politecnico di Torino, Turin, 10128, Italy

P. Marzocca[3]
Clarkson University, Potsdam, NY, 13699, USA

and

A. Behal[4]
University of Central Florida, Orlando, FL, 32826, USA

I. Introduction

The evaluation of the nonlinear flutter instability of slender wings represents a critical condition to test and validate control algorithm, [1-4] are case in point. On a benchmark 2D aeroelastic model several linear and nonlinear active controllers [5,6,7] as well as various adaptive control schemes [2,3,7,8] have been tested. In spite of the recent years' flourishing literature on aeroelastic adaptive controls, there is a noted lack of robustness and sensitivity analysis with respect to structural proprieties degradation which might be associated with a structural failure. Structural mode frequencies and aeroelastic response, including Limit Cycle Oscillations (LCOs) characteristics, are significantly affected by changes in stiffness. This leads to a great interest in evaluating and comparing the adaptation capabilities of different control architectures subjected to large plant uncertainties and unmodeled dynamics. The contribution of this technical note lies in the derivation and implementation of state feedback Model Reference Adaptive Control (MRAC) solutions for a 2D aeroelastic nonlinear system and in evaluating the robustness of different control strategies to damage leading to the deterioration of the structural stiffness characteristics. The Standard MRAC, a Modified MRAC, and the $\mathcal{L}_1$ adaptive controller are the three model-reference adaptive control solutions analyzed. The standard direct MRAC solution [9] serves as threshold to assess whether or not the

[1] Ph.D Candidate, Department of Mechanical and Aerospace Engineering, C.so Duca degli Abruzzi 24. Visiting Scholar in the Mechanical and Aeronautical Engineering Department at Clarkson University
[2] Associate Professor, Department of Mechanical and Aerospace Engineering, C.so Duca degli Abruzzi 24.
[3] Professor, Department of Mechanical and Aeronautical Engineering, 8 Clarkson Avenue.
[4] Associate Professor, Department of EECS and NanoScience Technology Center, 12424 Research Parkway Suite 400.

more complex algorithms are an effective improvement to it. Both Modified Model Reference [9] and $\mathcal{L}_1$ [10] adaptive controllers, which embody different modifications to the standard scheme with the intent to improve robustness and performance at the same time, are proposed in this work. For consistency of the analysis, all the adaptive scheme solutions are derived for the same control objective [11-14] and are applied to the same aeroelastic plant, which is a two-DOF structurally nonlinear plunging and pitching lifting surface in a quasi-steady aerodynamic flow. The model has pitch polynomial type structural nonlinearities and uses a single trailing-edge control surface. The proposed aeroelastic model exhibits a supercritical Hopf-bifurcation behavior, that is a stable Limit Cycle Oscillations (LCOs) obtained past the flutter speed [15]. Investigation results and pertinent comments on the adaptation performance and robustness of the three schemes are presented.

II. Aeroelastic Model

The classical wing-flap configuration used as benchmark for flutter suppression active controller testing and performance evaluation [11-15] is illustrated in Figure 1. The schematic shows the 2 Degrees-of-Freedom (DOF) aeroelastic systems with plunging and pitching displacements, with an attached trailing edge control surface. The plunging h (positive downward) and pitching α (measured from the horizontal at the elastic axis of the airfoil, positive nose up) displacements are restrained by a pair of springs attached to the elastic axis (EA) of the airfoil with spring constants, k_h and $k_\alpha(\alpha)$, respectively. Here, $k_\alpha(\alpha)$ denotes a continuous, linear parameterizable nonlinearity, that is, the aeroelastic system has a continuous nonlinear (5th-order) restoring moment in the pitch DOF. Such continuous nonlinear model for stiffness results from a thin wing or propeller subjected to large torsional amplitudes [5]. Similar models [3,11,15,16] have been examined and provide a basis for comparison. The aerodynamically unbalanced control surface deflection β is measured from the axis created by the airfoil at the control flap hinge and is positive for flap down. While this flap is primarily used to initiate and terminate maneuvers, it is considered here as a means of suppressing aeroelastic instabilities. As already indicated earlier, the same plant is used to test the three different adaptive control strategies and their ability to respond to structural degradation simulated by suddenly reducing stiffness values.

The equations of motion for the 2DOF aeroelastic system under consideration are given as [1,15].

$$\begin{bmatrix} \mathrm{m} & \mathrm{m}x_a b \\ \mathrm{m}x_a b & \mathrm{I}_\alpha \end{bmatrix} \begin{bmatrix} \ddot{\mathrm{h}} \\ \ddot{\alpha} \end{bmatrix} + \begin{bmatrix} \mathrm{c}_\mathrm{h} & 0 \\ 0 & \mathrm{c}_\alpha \end{bmatrix} \begin{bmatrix} \dot{\mathrm{h}} \\ \dot{\alpha} \end{bmatrix} + \begin{bmatrix} \mathrm{k}_\mathrm{h} & 0 \\ 0 & \mathrm{k}_\alpha(\alpha) \end{bmatrix} \begin{bmatrix} \mathrm{h} \\ \alpha \end{bmatrix} = \begin{bmatrix} -\mathrm{L} \\ \mathrm{M} \end{bmatrix} \tag{1}$$

where m is the mass of the airfoil, x_a the dimensionless distance measured from the elastic axis to the center of mass, I_α the mass moment of inertia of airfoil about elastic axis, $\mathrm{C}_\mathrm{h}, \mathrm{C}_\alpha$ the structural damping coefficients in plunging and pitching and the lift L and aerodynamic moment M are modeled in their quasi-steady form as

$$\mathrm{L} = \rho U^2 b c_{l\alpha} \left[\alpha + \frac{\dot{\mathrm{h}}}{U} + \left(\frac{1}{2} - a\right) b \left(\frac{\dot{\alpha}}{U}\right)\right] + \rho U^2 b c_{l\beta} \beta$$

$$\mathrm{M} = \rho U^2 b^2 c_{m\alpha} \left[\alpha + \frac{\dot{\mathrm{h}}}{U} + \left(\frac{1}{2} - a\right) b \left(\frac{\dot{\alpha}}{U}\right)\right] + \rho U^2 b^2 c_{m\beta} \beta \tag{2}$$

where U is the free stream velocity, c_{l_α} c_{m_β} c_{l_β} c_{m_β} are lift and moment coefficients respectively of the airfoil and the control surface; a is the dimensionless distance between the mid-chord and the elastic axis and b is the semi-chord of airfoil. Equations (1) can be written into the equivalent state-space form:

$$\dot{\mathrm{z}} = \mathrm{f}(\mathrm{z}) + \mathrm{g}(\mathrm{z})\beta, \qquad \mathrm{y} = [\mathrm{z}_2\ \mathrm{z}_4] \tag{3}$$

where $\mathrm{z}(\mathrm{t}) = [\mathrm{z}_1\ \mathrm{z}_2\ \mathrm{z}_3\ \mathrm{z}_4]^\mathrm{T} \triangleq \left[\mathrm{h}\ \alpha\ \dot{\mathrm{h}}\ \dot{\alpha}\right]^\mathrm{T}$ is the system states vector, $\beta(t) \in \mathrm{R}^1$ is a flap deflection control input, $\mathrm{y}(\mathrm{t}) \in \mathrm{R}^2$ denotes the designated output, and $\mathrm{f}(\mathrm{z})$ and $\mathrm{g}(\mathrm{z}) \in \mathrm{R}^1$ assume the following form:

$$\mathrm{f}(\mathrm{z}) = \begin{bmatrix} \mathrm{z}_3 \\ \mathrm{z}_4 \\ -\mathrm{k}_1\mathrm{z}_1 - [\mathrm{k}_2\mathrm{U}^2 + \mathrm{p}(\mathrm{z}_2)]\mathrm{z}_2 - \mathrm{c}_1\mathrm{z}_3 - \mathrm{c}_2\mathrm{z}_4 \\ -\mathrm{k}_3\mathrm{z}_1 - [\mathrm{k}_4\mathrm{U}^2 + \mathrm{p}(\mathrm{z}_2)]\mathrm{z}_2 - \mathrm{c}_2\mathrm{z}_3 - \mathrm{c}_4\mathrm{z}_4 \end{bmatrix}; \qquad \mathrm{g}(\mathrm{z}) = \begin{bmatrix} 0 \\ 0 \\ \mathrm{g}_3\mathrm{U}^2 \\ \mathrm{g}_4\mathrm{U}^2 \end{bmatrix}, \quad \mathrm{g}_4 \neq 0 \tag{4}$$

where $\mathrm{p}(\mathrm{z}_2)$ and $\mathrm{q}(\mathrm{z}_2) \in \mathrm{R}^1$ are continuous, linear parameterizable nonlinearities in the output variable resulting from the nonlinear pitch spring constant $\mathrm{k}_\alpha(\alpha)$. The set of constant k_i and c_i $\forall \mathrm{i} = 1, \ldots 4$, as well as g_3 and g_4 are defined and reported in [2]; $\mathrm{g}(\mathrm{z})$ consists of constants, and partitioning $\mathrm{f}(\mathrm{z})$ in the constant and variable part, the aeroelastic system to be controlled belongs to a class of plant described by

$$\dot{\mathrm{x}}(\mathrm{t}) = A\mathrm{f}(\mathrm{x}, \mathrm{t}) + \mathrm{Bu}(\mathrm{t}) \tag{5}$$

where A and B are constant, $\mathrm{f}(\mathrm{x}, \mathrm{t})$ is a nonlinear function, and $\mathrm{u}(\mathrm{t})$ is the control signal.

For control law design purpose, the unknown component of the state matrix and the nonlinear function Eq.(5) can be decomposed from the known part as follow:

$$A = A^* + \Delta A; \quad f(x,t) = f^*(x,t) + \Delta f(x,t); \quad B = B^* + \Delta B \tag{6}$$

where the superscript * denotes the nominal values and $\Delta A, \Delta f(x,t)$ and ΔB denote the uncertain portions of A, $f(x,t)$ and B, respectively. Hence, the dynamic system equation (5) can be expressed as

$$\dot{x}(t) = A^* f(x,t) + \big(\Delta A + \Delta f(x,t)\big) + (B^* + \Delta B)u(t). \tag{7}$$

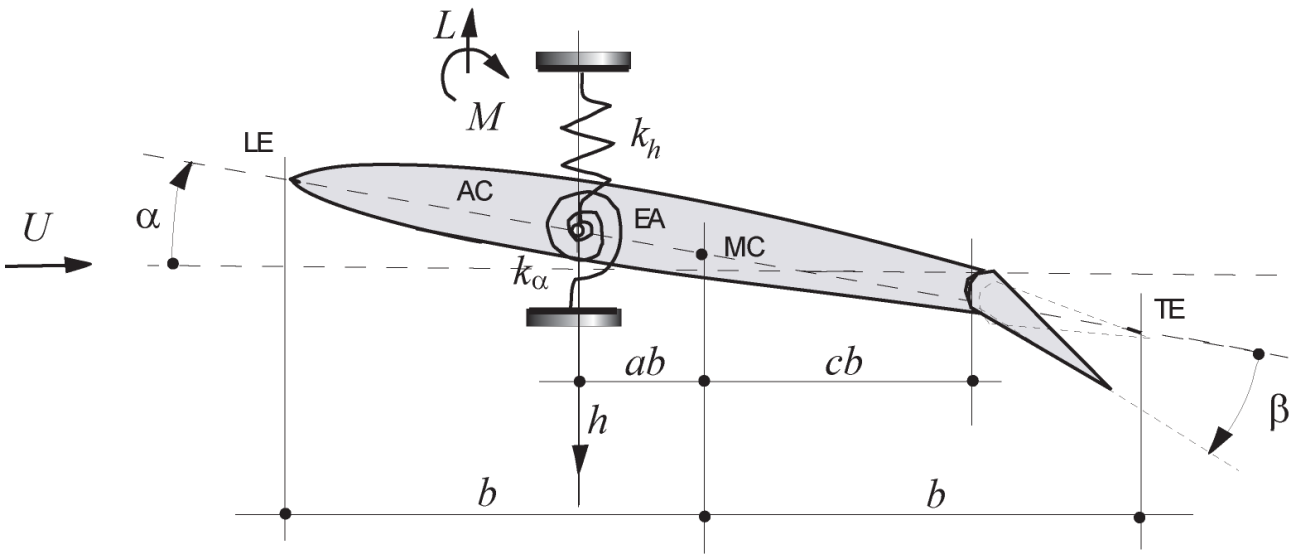

Figure 1 2D *wing section schematic*

III. Adaptive Control Architectures: Control Objective and Problem formulations

The control objective is to suppress the aeroelastic oscillatory motion of the system by driving the pitch angle α to a constant set point, typically zero degrees, while adaptively compensating for uncertainties in all parameters of the model and the nonlinearity. In this particular development, it is assumed that the only available states for feedback are $x_{meas} = [\alpha\ \dot{\alpha}]$. If the pitch regulation is achieved, the plunging motion is damped-out [1-4]. Three different model-reference adaptive control architectures are introduced and compared to evaluate the effectiveness of modifications from the standard MRAC scheme. The aeroelastic system equations are rewritten into amenable form as to fit the problem formulation for each control scheme. A detailed description of the various architectures, control, and adaptive laws is supplied next to highlight the differences between them.

A. Standard MRAC solution

Equation (7) describes a class of plants that is usually written in the following form amenable to model reference control scheme

$$\dot{x}(t) = A_m x(t) + B\theta^{*^T} x(t) + Bu(t) \tag{8}$$

where $x \in \mathbb{R}^n$ is the state vector, assumed to be measurable, $u \in \mathbb{R}$ is the control input, $\theta^* \in \mathbb{R}^n$ is an unknown parameters vector belonging to a known compact convex set $\Omega \subset \mathbb{R}^n$, $A_m \in \mathbb{R}^{n\times n}$ is Hurwitz [17] and $B \in \mathbb{R}^n$ are known and the pair $(A_m; B)$ is controllable. As proved in [9], the fact that the parameter θ^* appears linearly in Eq. (8) does not mean that the dynamics are linear. For a standard MRAC scheme, the control problem lies in choosing $u(t)$ such that all the states $x(t)$ in the closed-loop system are uniformly bounded and track the state vector of a desired reference model

$$\dot{x}_m(t) = A_m x_m(t) + B_m r(t), \qquad x_m(0) = x_0 \tag{9}$$

both in transient and in steady-state for any bounded reference signal $r(t)$. The standard MRAC solution to this problem is based on the states error between the plant and the reference model [9] defined as

$$e(t) = x(t) - x_m(t) \tag{10}$$

from which the unknown parameter vector $\theta^*(t)$ is estimated by

$$\dot{\hat{\theta}}(t) = \text{proj}\left(\Gamma e^T(t) P b x(t)\right), \quad \hat{\theta}(0) = \hat{\theta}_0 \in \Omega \tag{11}$$

and the associated control law is

$$u(t) = -\hat{\theta}^T(t) x(t) + k_0 r(t) \tag{12}$$

where $\hat{\theta}(t)$ is the estimate of the unknown parameters $\theta^*(t)$. $\Gamma > 0$ is the adaptive gain, e is the tracking error, and $P = P^T > 0$ is the solution of the Lyapunov equation $PA_m + A_m^T P = -I$. The projection operator is used to constrain $\hat{\theta}(t)$ inside the compact set Ω for all t and is defined in [9,10]. For the particular application considered the reference signal $r(t)$ is simply a constant set point, the elastic response has to damp-out with time to zero, which reduces the system to a regulation problem. The controller design parameters for the reference model are selected as follows:

$$A_m = \begin{bmatrix} 0 & 1 \\ -0.3 & -1 \end{bmatrix}; \; B_m = \begin{bmatrix} 0 \\ 4 \end{bmatrix}; x_0 = \begin{bmatrix} 0 \\ 0.1 \end{bmatrix}; \; r(t) = 0 \tag{13}$$

while the adaptive law parameters are

$$P = 500I; \Gamma = 10;\ B = \begin{bmatrix} 1 \\ 0.1 \end{bmatrix}; \Omega \in [-5; 5];\ \hat{\theta}(0) = \begin{bmatrix} 0 \\ 0 \end{bmatrix}; \tag{14}$$

B. $\mathcal{L}_1$ adaptive controller: State feedback in the presence of matched uncertainties

The $\mathcal{L}_1$ control problem formulation has the same standard MRAC form, since it is defined as a tracking problem between the system dynamics (8) and the reference model dynamics (9). However, the solution, whose detailed derivation can be found in [10], slightly differs being based on a state predictor error

$$\tilde{x}(t) = x(t) - \hat{x}(t) \tag{15}$$

instead of the tracking error as in (10). The state predictor dynamics is given by

$$\dot{\hat{x}}(t) = A_m\hat{x}(t) + B(\hat{\theta}^T(t)x(t) + u(t), \qquad \hat{x}(0) = x_0, \tag{16}$$

where A_m is the same Hurwitz matrix in (9), $\hat{x}(t)$ are the predicted states, $x(t)$ are the actual system states, $u(t)$ is the control signal and $\hat{\theta}$ is again the unknown parameters estimation computed by the adaptive law

$$\dot{\hat{\theta}}(t) = \text{proj}\left(\Gamma\tilde{x}^T(t)Pbx(t)\right), \quad \hat{\theta}(0) = \hat{\theta}_0 \in \Omega \tag{17}$$

The associate control law is defined as

$$u(t) = C(s)[-\hat{\theta}^T(t)x(t) + k_0 r(t)] \tag{18}$$

where $C(s)$ is a stable strictly proper transfer function, with $C(0) = 1$. This is a first-order low-pass filter, which assumes the form

$$C(s) = \frac{1}{ks + 1} \tag{19}$$

with $k > 0$ being the design parameter. To guarantee stability and convergence, the condition $\|W_b(s)(C(s) - 1)\|_1\theta_{max} < 1$ must be respected, where $W_b(s) = (sI - A_m)^{-1}B$ and θ_{max} is an upper bound for $\left\|\hat{\theta}\right\|_1$. Γ and P have the same meaning as in (11). However, contrary to the MRAC theory [9], the adaptive gain Γ in the $\mathcal{L}_1$ adaptive scheme is not subject to any stability constraint, because of the decoupling of the adaptive law dynamics from the system dynamics operated by the filter, in that particular location of the architecture. This allows the designer to increase Γ to very high

values for fastness, without affecting the controller robustness [10]. On these theoretical bases, the controller design parameters, have been selected as follows:

$$k = 0.015; \qquad A_m = \begin{bmatrix} 0 & 1 \\ -0.3 & -1 \end{bmatrix}; \qquad B = \begin{bmatrix} 1 \\ 0.1 \end{bmatrix}; \qquad x_0 = \begin{bmatrix} 0 \\ 0.1 \end{bmatrix}; \tag{20}$$

$$P = 500I; \Gamma = 10^7; \ \Omega \in [-5; 5]; \ \hat{\theta}(0) = \begin{bmatrix} 0 \\ 0 \end{bmatrix}; \tag{21}$$

where the reference model state and control matrices, as well as the convex set of the adaptive parameters and P are maintained equal to (13), for consistency of the analysis. Herein, the filter was tuned by trial and error and the adaptive gain was set high as suggested in [10].

C. Modified MRAC with normalized adaptive laws and transient performance improvement

It is worthwhile introducing in this investigation another MRAC architecture, which involves signal filtering, but in a different location of the control architecture. This is known as modified MRAC for performance improvement [9, 18]. The problem formulation is still a model reference-tracking problem; however, the controller derivation is based on a parametric expression of (8) and the adaptive and control laws work on normalized signals, which increase the robustness of this scheme. Equation (8) can be rewritten as

$$x(t) = W_b(s)\left[\theta^{*T} x(t)\right] + W_b(s)[u(t)] \tag{22}$$

where $W_b(s) = (sI - A_m)^{-1}B$ Based on (A_m, B) controllability, a vector $c_0 \in \mathbb{R}^n$ is defined so that $W_m(s) \triangleq c_0^T W_b(s)$ is a strictly proper minimum-phase transfer function. The parametric expression of the model is consequently written as

$$z(t) = \theta^{*T} \phi(t) \tag{23}$$

where $z(t) = C_0^T x(t) - W_m(s)[u(t)]$ and $\phi(t) = W_m(s)[x(t)]$ are available for measurements. The structure and parameters of the unmodeled dynamics are assumed unknown. Performance improvement is obtained by enriching the control signal with an auxiliary input u_a, which involves the above mentioned feedback signal filtering

$$u(t) = -\hat{\theta}^T(t)x(t) + k_0 r(t) + u_a(t) \tag{24}$$

where

$$u_a(t) = -Q(s)\left[\epsilon m_s^2 + W_{c_0}(s)[\,W_b(s)[x^T(t)]\dot{\hat{\theta}}(t)]\right] \tag{25}$$

Herein $W_{c_0}(s) = -c_0^T(sI - A_m)^{-1}$, $Q(s) = W_m(s)^{-1}/(\tau s + 1)^{n^*}$, and n^* is the relative degree of $W_m(s)$, while $\tau > 0$ is a design parameter. The associated adaptive law is expressed as

$$\dot{\hat{\theta}}(t) = \text{proj}\big(P(t)\epsilon(t)\phi(t)\big), \qquad \hat{\theta}(0) = \hat{\theta}_0 \in \Omega \tag{26}$$

$$\dot{P}(t) = -P(t)\frac{\phi(t)\phi^T(t)}{m_s^2}P(t), \qquad P(0) = P_0 \tag{27}$$

where ϵ is the estimation error and is defined as $\epsilon(t) = \frac{\left(z(t) - \hat{\theta}^T\phi(t)\right)}{m_s^2}$. The normalizing signal is $m_s^2(t) = 1 + \phi^T(t)\phi(t)$, and it is designed to guarantee boundedness of $\left|\frac{\phi(t)}{m_s(t)}\right|$, independently whether $\phi(t)$ is bounded or not. It must be noticed that, in this formulation, P is a function of t and not a constant matrix. Stability and convergence proof of this robust adaptive law are reported in [9]. For consistency, the reference model state matrix, the initial conditions, $\hat{\theta}$ convex set and $P(0)$ are set identical to the other control schemes, while the different design parameters are set as follows

$$\tau = 0.5; \qquad c_0 = \begin{bmatrix}1\\1\end{bmatrix}; \tag{28}$$

It can be noticed that the filter $Q(s)$ has a similar expression to $C(s)$. However, since it appears in a different location of the control schemes and operates on different signals, the two behaviors are fundamentally different as shown in the results section.

IV. Simulation Results

To verify the control algorithms performance and their robustness and adaptive capabilities, an extensive set of simulations is carried out with the 2DOF plunging and pitching aeroelastic model with trailing edge control surface, in several conditions within a parameters region of interest. The proposed aeroelastic plant, whose parameters are reported in Table 1 [15], shows an LCO behavior at the critical wind speed $U_{\text{flutter}} = 7\ \text{m/s}$ in nominal condition, which drops down to $5\ \text{m/s}$ when the failure is simulated. The trust region of the quasi-steady aerodynamic model stays within a range of angle of attack up to 10 degrees. For this reason, the wind speed increment and the structural failures applied to the plant are modulated so that the resulting LCOs motion is bounded inside the valid angle

of attack domain. In particular, failure is simulated by a 50% reduction of the stiffness matrix K nominal value and the post-flutter velocity is 30% higher the flutter speed, $U_{\text{post-flutter}} = 9\text{m/s}$. The plunging/pitching phase-diagrams of the aeroelastic system subject to non-nominal conditions are reported in Figure 2, in which the effect on the LCOs features are noticeable. Figures 2 and 3 together show how the post-flutter wind speed and the stiffness reduction lead to different dynamic behaviors, in terms of frequencies and amplitude in both DOFs, that are worth to be evaluated, and represent a valid test for the control scheme adaptability.

Table 1 ***2D Aeroelastic Plant Parameters***

a, b	$-0.4, 0.135\ (m)$	$c_{l_\alpha}, c_{m_\alpha}$	$6.28, (0.5 + a)c_{l_\alpha}$
$\mathrm{k}_\alpha(\alpha), \mathrm{k}_\mathrm{h}$	$\sum_{i=1}^{5} \tau_i \alpha^{i-1}, 2844.4\ (N \cdot m^{-1})$	c_{l_β}, c_{m_β}	$3.358, -0.635$
ρ	$1.225\ (Kg \cdot m^3)$	m	$12.387\ kg$
τ_i	$[2.8\ \ -62.3\ \ 3709.7\ \ -24{,}195.6\ \ 48{,}756.9]^T$	I_α	$0.065\ (kg \cdot m^2)$
$\mathrm{c}_\alpha, \mathrm{c}_\mathrm{h}$	$0.036\ (N \cdot s),$ $27.43\ (N \cdot m^{-1} \cdot s^{-1})$	x_α	$[0.0873 - (b + ab)]/b$

Testing and verification of the adaptive control schemes is carried out by perturbing the aeroelastic system with an initial pitch angle $\alpha(0) = 0.1$ [rad] and monitoring the controller as well as the plunging and pitching responses evaluated in the simulation environment. The wind speed range of interest is $U = 7$ to $9\ (\text{m/s})$ while the plunging and pitching stiffness range of interest are $\mathrm{K} = \mathrm{K}_{\text{nom}}$ to $\mathrm{K}_{\text{nom}}/2$. A selection of the most meaningful results is reported in this note, despite the extensive number of simulations performed. In particular, the aeroelastic response for the cases reported in Table 2, are presented in the following representative figures. Each case is characterized by the closed loop wind speed U_{CL}, the plant stiffness matrix value K, the controller activation time t_{ON} and the open-loop flutter speed of the actual configuration $U_{\text{flutter}_{\text{OL}}}$. It is noted that, for the combined post-flutter and reduced stiffness condition, the system is controlled only at 0 sec to avoid unreasonable values of the pitch angle. The numerical integration in all the simulations is performed using a fourth-order Runge-Kutta with a sampling time $\mathrm{t}_\mathrm{s} = 0.001$ sec .

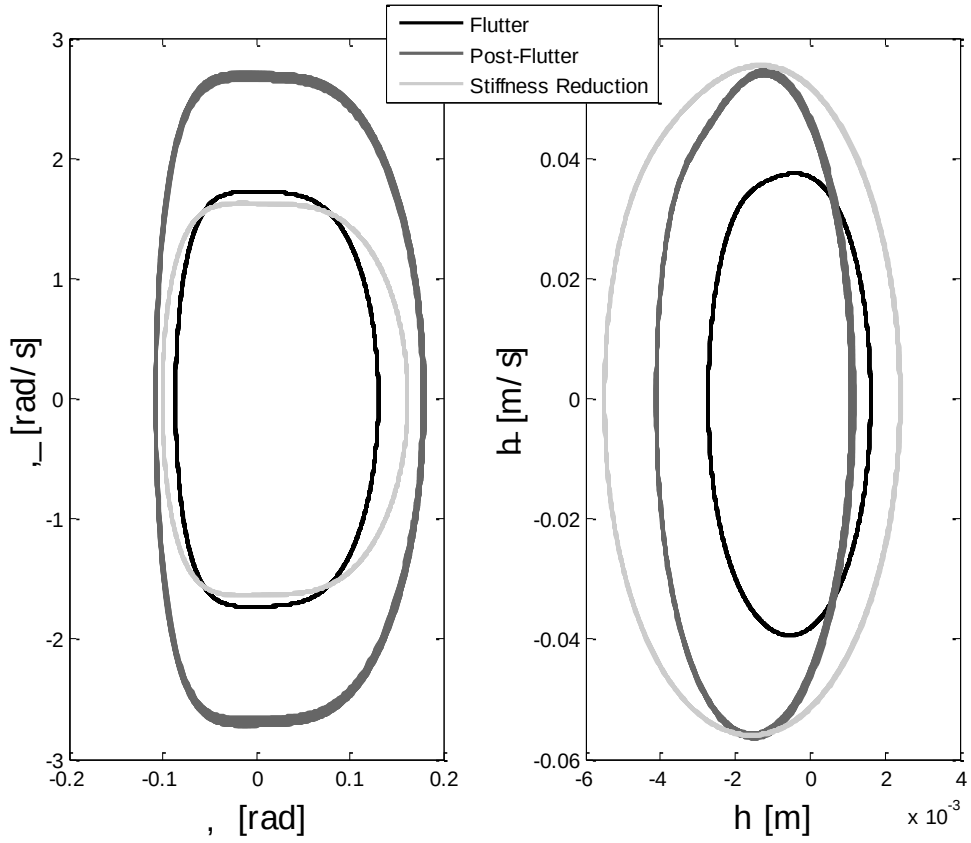

Figure 2 ***Aeroelastic System Phase Diagrams***

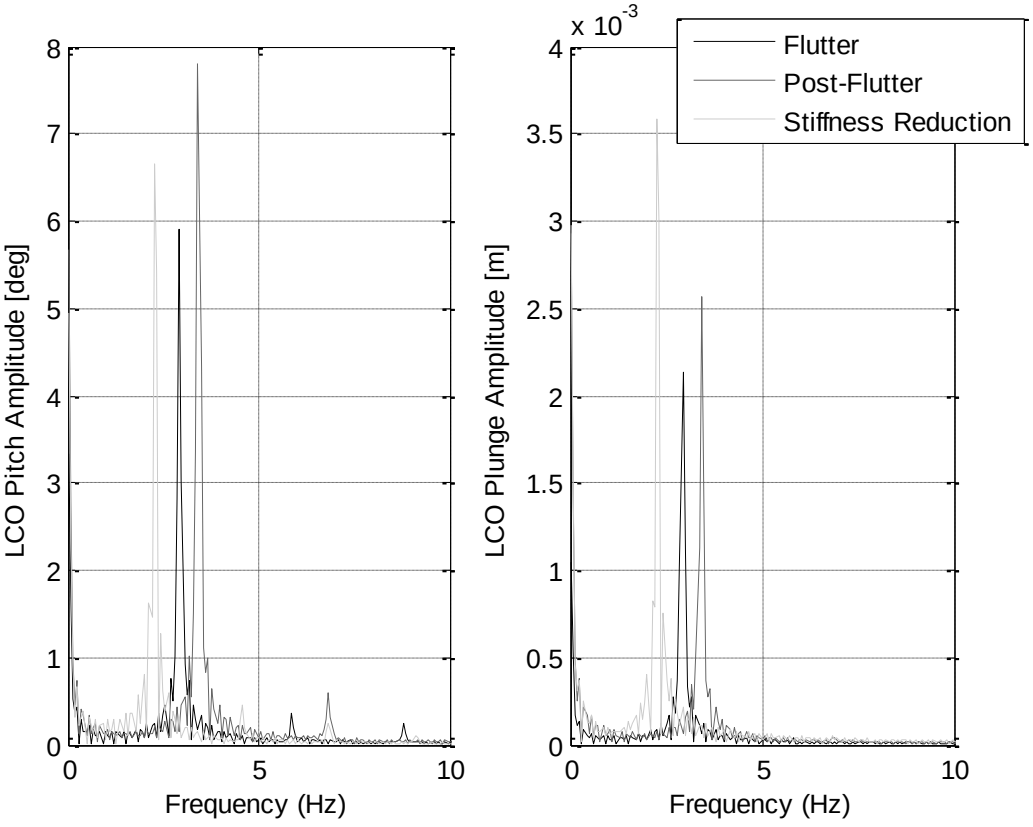

Figure 3 ***Aeroelastic System LCOs frequency spectra at different conditions***

Table 2 ***Simulations Cases***

	Case 1	**Case 2**	**Case 3**	**Case 4**	**Case 5**	**Case 6**	**Case 7**
$\boldsymbol{U_{\mathrm{CL}}}$	$7\ m/s$	$7\ m/s$	$7\ m/s$	$7\ m/s$	$9\ m/s$	$9\ m/s$	$9\ m/s$
K	K_{nom}	K_{nom}	$\frac{K_{nom}}{2}$	$\frac{K_{nom}}{2}$	K_{nom}	K_{nom}	$\frac{K_{nom}}{2}$
$\boldsymbol{t_{ON}}$	$0\ sec$	$10\ sec$	$0\ sec$	$10\ sec$	$0\ sec$	$10\ sec$	$0\ sec$
$\boldsymbol{U_{\mathrm{flutter_{OL}}}}$	$7\ m/s$	$7\ m/s$	$5\ m/s$	$5\ m/s$	$7\ m/s$	$7\ m/s$	$5\ m/s$

Firstly, Figures 5 through 10 show that the problem is well posed since all the adaptive schemes are able to control the system, independently from the activation time of the controller (LCOs induced or not). The robustness and adaptive capability of each individual control scheme is hereafter discussed. Despite the relevant variations in the aeroelastic system dynamic (LCOs frequency and amplitude) due to the imposed conditions, the convergence time of each control scheme does not deteriorate noticeably during the tests. Standard MRAC, as expected, shows slow adaptation rate and subsequently poor performance in time response, about 10 sec, when activated at time zero, see Figs. 4(b), 6(b), 8(b), and 10(b). On the other hand, the MRAC scheme exhibits a faster behavior, about 1 sec, when activated at time 10 sec, with fully established LCOs, see Figs. 4(c), 6(c), and 8(c). This is due to the presence, in this last condition, of a higher $\dot{\alpha}$ that enriches the feedback signal, reducing the convergence time. A quite similar response is observed for the $\mathcal{L}_1$ control scheme, as illustrated in Figs. 4(d-e), 6(d-e), 8(d-e), and 10(d). The only perceivable difference, from the standard MRAC response, is the introduction of high frequency oscillations in the control signal, as reported in Fig. 5(d-e), 5(d-e), 9(d-e), and 10(e). These oscillations derive from the adaptive law computation algorithm, as shown in Fig. 11(b), whose differential equation is made too stiff by the extremely high value of the adaptive gain Γ and propagate, mildly damped by the filter and the system dynamic, in the observed state. The effect is reduced for LCO induced conditions, when activation time is after 10 sec, always for the presence of a higher $\dot{\alpha}$ which help the adaptation law to a faster convergence. Subplots (f-g) of Figures 4 through10 report the system response and the control command time-

histories when the plant is controlled by the Modified MRAC scheme. It shows a fast, about 1.5 sec, and robust response that does not depend on the activation time. Smooth convergence of the adaptive parameters is verified through the entire simulation test campaign, Fig. 11 (c) is an example. A drawback of the Modified MRAC scheme is that it has the highest overshoot among the all three control methods, so that command saturation is often reached Fig 5(f-g), 7(f-g), 9(f), and 10(g). This is caused by the adjunct control signal u_a of Eq. (22), whose primary function is to enrich the signal for faster response and reduced tracking error. To conclude, the standard MRAC and the $\mathcal{L}_1$ control have shown reduced robustness with respect to the Modified MRAC scheme, presenting a different response either faster or slower as function of the activation time, that is the controlled state value at the controller activation. This is also due, in addition to the already mentioned beneficial effect of the state derivative feedback, to the dependency of the unknown parameters estimation law from the state error $\mathrm{e(t)}$ (MRAC) or $\tilde{\mathrm{x}}\mathrm{(t)}$ ($\mathcal{L}_1$). The closer the actual states are to the reference model or the state estimator states, the faster is the response. This effect can be appreciated in all the control schemes response, being reference model control architectures by definition, but it is strongly reduced in the Modified MRAC scheme by the presence of the enriched signal u_a.

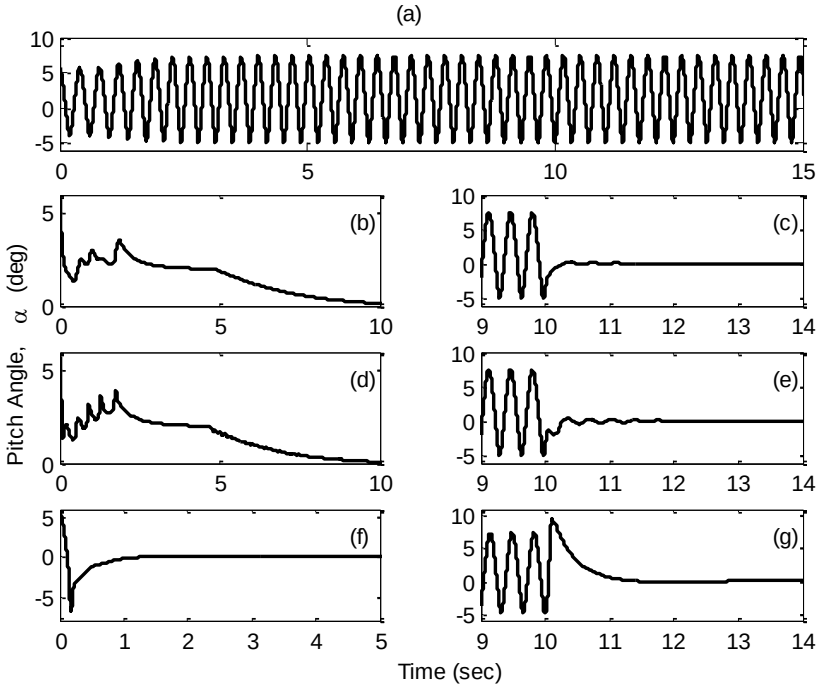

Figure 4 ***Nominal Flutter Condition Responses*: $U_{flutter}$, K_{nom} (*Case 1, 2); (a) Uncontrolled System; (b) Standard MRAC (ON at 0 sec); (c) Standard MRAC (ON at 10 sec); (d) L1 (ON at 0 sec); (e) L1 (ON at 10 sec); (f) Modified MRAC (ON at 0 sec); (g) Modified MRAC (ON at 10 sec)***

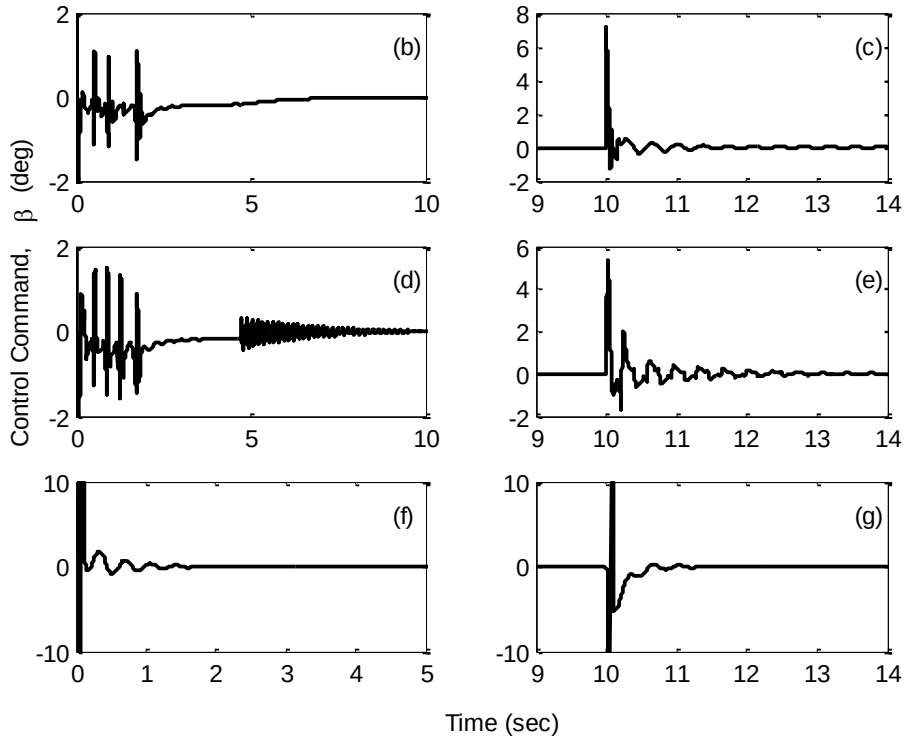

Figure 5 ***Nominal Flutter Condition, Control Command Time Histories*: $U_{flutter}$, K_{nom} (*Case 1, 2); (b) Standard MRAC (ON at 0 sec); (c) Standard MRAC (ON at 10 sec); (d) L1 (ON at 0 sec); (e) L1 (ON at 10 sec); (f) Modified MRAC (ON at 0 sec); (g) Modified MRAC (ON at 10 sec)***

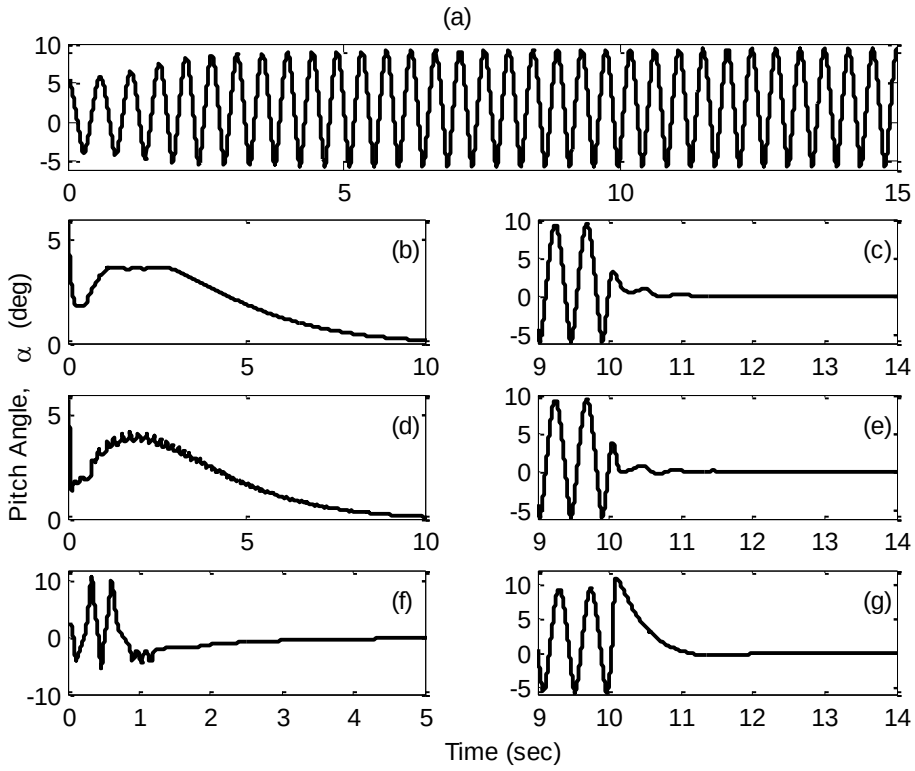

Figure 6 ***Stiffness Reduction Condition Responses*: $U_{flutter}$, $K_{reduced}$ (*Case 3, 4); (a) Uncontrolled System; (b) Standard MRAC (ON at 0 sec); (c) Standard MRAC (ON at 10 sec); (d) L1 (ON at 0 sec); (e) L1 (ON at 10 sec); (f) Modified MRAC (ON at 0 sec); (g) Modified MRAC (ON at 10 sec)***

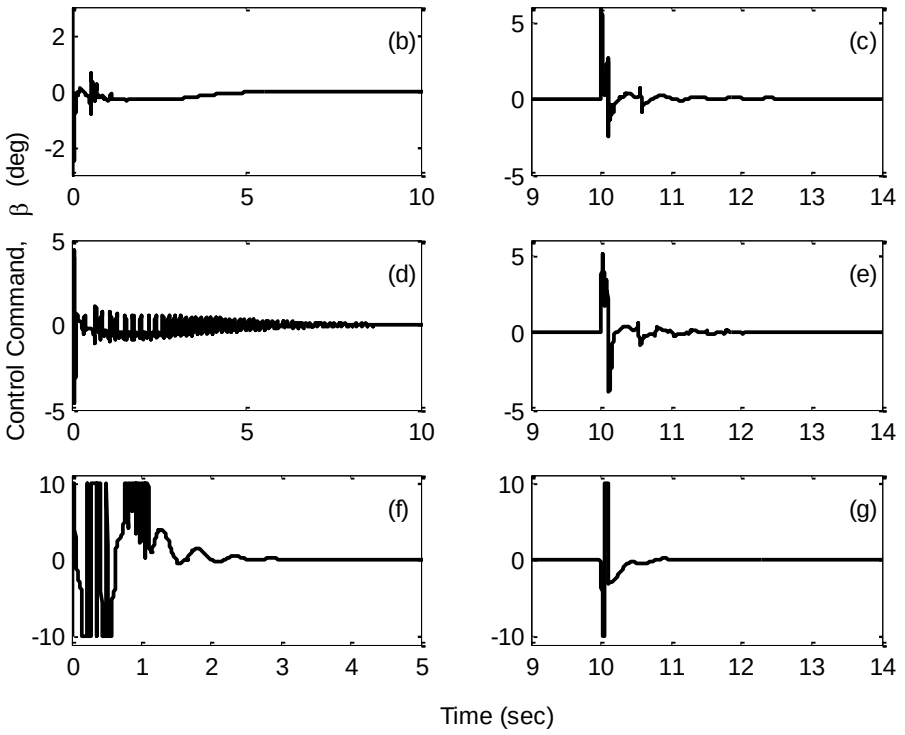

Figure 7 ***Stiffness Reduction Condition, Control Command Time Histories*: $U_{flutter}$, $K_{reduced}$ (*Case 3, 4); (b) Standard MRAC (ON at 0 sec); (c) Standard MRAC (ON at 10 sec); (d) L1 (ON at 0 sec); (e) L1 (ON at 10 sec); (f) Modified MRAC (ON at 0 sec); (g) Modified MRAC (ON at 10 sec)***

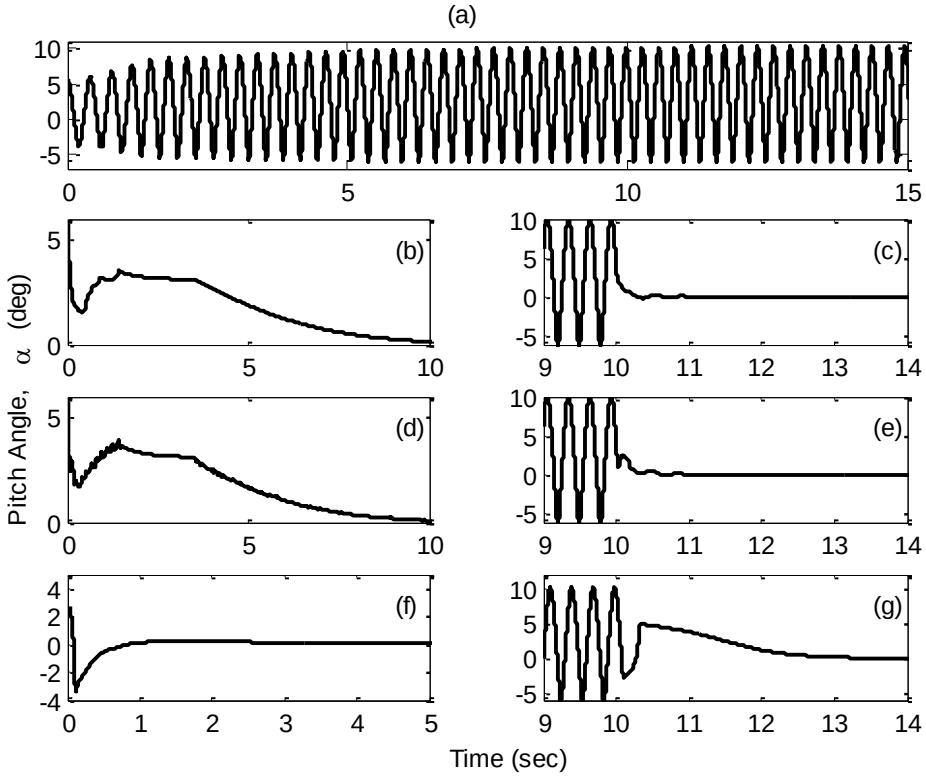

Figure 8 ***Post-Flutter Speed Condition Responses*: $U_{post-flutter}$, K_{nom} (*Case 5, 6); (a) Uncontrolled System; (b) Standard MRAC (ON at 0 sec); (c) Standard MRAC (ON at 10 sec); (d) L1 (ON at 0 sec); (e) L1 (ON at 10 sec); (f) Modified MRAC (ON at 0 sec); (g) Modified MRAC (ON at 10 sec)***

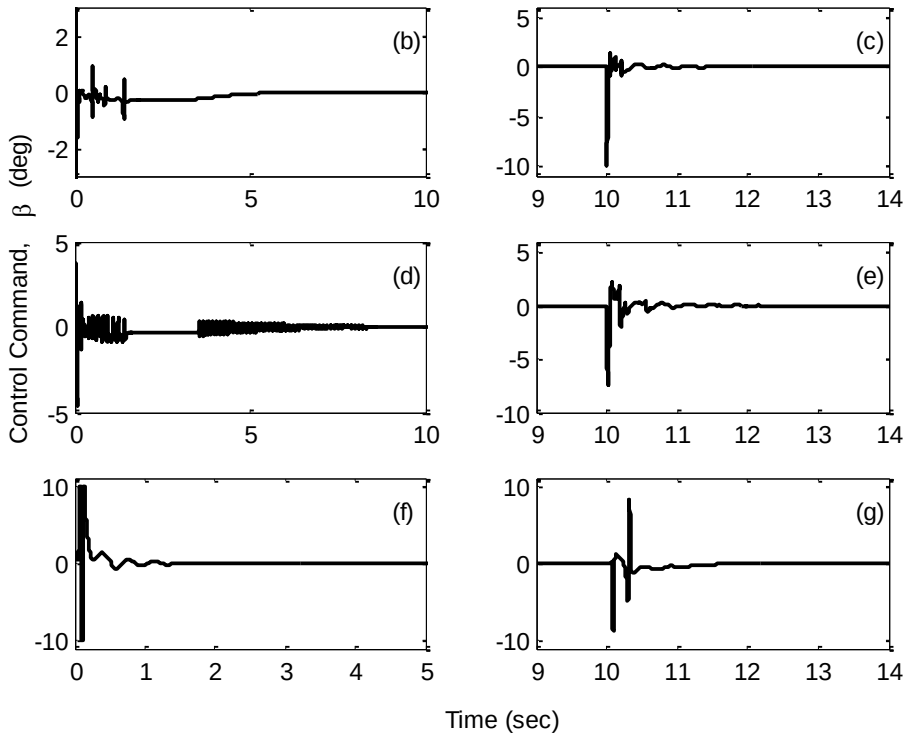

Figure 9 ***Post-Flutter Speed Condition, Control Command Time Histories*: $U_{post-flutter}$, K_{nom} (*Case 5, 6); (b) Standard MRAC (ON at 0 sec); (c) Standard MRAC (ON at 10 sec); (d) L1 (ON at 0 sec); (e) L1 (ON at 10 sec); (f) Modified MRAC (ON at 0 sec); (g) Modified MRAC (ON at 10 sec)***

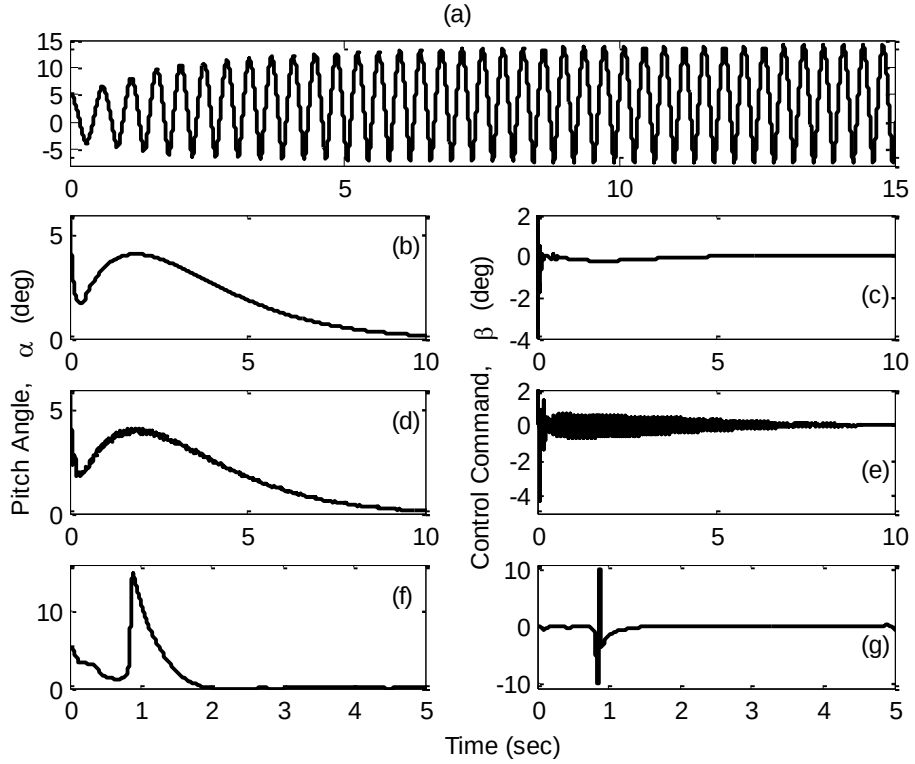

Figure 10 ***Combined Condition Responses and Control Command Time Histories*: $U_{post-flutter}$, $K_{reduced}$, *controller ON at 0 sec* (*Case 7); (a) Uncontrolled System; (b) Standard MRAC (α); (c) Standard MRAC (u); (d) L1 (α); (e) L1 (u); (f) Modified MRAC (α); (g) Modified MRAC (u)***

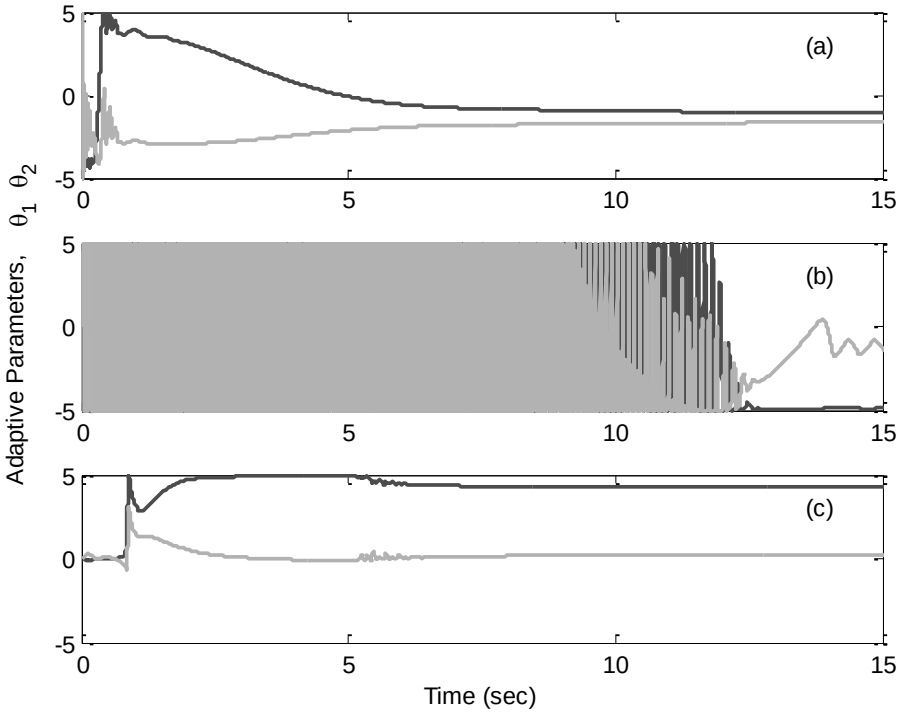

Figure 11 ***Adaptive Parameters example during simulation (case 7)***

V. Conclusions

In this technical note, a comparative analysis of three different model reference adaptive control schemes is carried out with the aim of evaluating their performance in suppressing aeroelastic instabilities in the presence of model uncertainties with the deterioration of structural stiffness characteristics. A 2D nonlinear aeroelastic plant is used for the controller testing purpose. For consistency, all the controllers have the same input-output architecture and all the design parameters are set to be identical. The effectiveness and robustness of all the adaptive schemes has been tested controlling the plant in nominal flutter condition first, and then by simulating a failure causing an instantaneous plunging/pitching stiffness reduction at a wind speed about 1.3 times the flutter velocity. Flutter and post-flutter suppression capabilities are investigated with the use of the three adaptive schemes. The extensive simulation campaign proved that only the Modified Model Reference Adaptive Control (Modified MRAC) is an effective improvement of the standard scheme in terms of both robustness and adaptation rate. However, as a drawback, it presents the highest overshoot among the all three control methods, so that command saturation is a concern and is likely to be reached. Unexpectedly, the $\mathcal{L}_1$ control scheme did not represent an effective improvement to the

standard scheme. For the application at hand, it has the same level of robustness of the comparative standard scheme, coupled with a not beneficial oscillatory behavior of the adaptive law solver, which reflects the oscillations to the control signal. Moreover, contrary to the standard scheme, which does not require any tuning operation, the $\mathcal{L}_1$ filter needed to be tuned by trial and error, which negatively affects the adaptation capabilities of the architecture. In addition, the proposed work serves as validation of the general effectiveness of model reference algorithms in handling system uncertainties and unmodeled dynamics. Preserving control capabilities in spite of significant structural failures is a valuable result that is worth to further investigation.

Acknowledgments

The authors would like to thank the EU Research Executive Agency (REA) for supporting the A2 Net Team project under FP7 Marie Curie Grant 269190. The A2 Net Team project established a connection among the authors and created an environment in which the authors have done much of the work presented here. The School of Engineering of Clarkson University also provided partial support for this research.

References

[1] Ko, J., Kurdila, A. J., and Strganac, T.W., "Nonlinear Control of a Prototypical Wing Section with Torsional Nonlinearity," *Journal of Guidance, Control, and Dynamics*, Vol. 20, No. 6, 1997, pp. 1181–1189. doi: 10.2514/2.4174.

[2] Behal, A., Marzocca, P., Rao, V.M., and Gnann, A.," Nonlinear Adaptive Control of an Aeroelastic Two-Dimensional Lifting Surface", *Journal of Guidance, Control, and Dynamics*, Vol. 29, No. 2, March-April 2006, pp. 382-390. doi: 10.2514/1.14011.

[3] Cassaro, M., Battipede, M., Cestino, E., Marzocca, P., Behal, A., "$\mathcal{L}_1$ adaptive flutter suppression control strategy for highly flexible structure", *SAE Int. J. Aerosp*., Vol. 6, No. 2, December 2013. doi: 10.4271/2013-01-2263.

[4] Singh, S.N., and Wang, L., "Output Feedback Form and Adaptive Stabilization of a Nonlinear Aeroelastic System," *Journal of Guidance, Control, and Dynamics*, Vol. 25, No. 4, 2002, pp. 725–732. doi: 10.2514/2.4939.

[5] Edwards, J.W., "Unsteady Aerodynamic Modeling and Active Aeroelastic Control," Guidance and Control Lab., Dept. of Aeronautics and Astronautics, SUDARR 504, Stanford Univ., Stanford, CA, Feb. 1977; also NASA CR-148019, 1977.

[6] Block, J.J., and Strganac, T.W., "Applied Active Control for a Nonlinear Aeroelastic Structure," *Journal of Guidance, Control, and Dynamics*, Vol. 21, No. 6, 1998, pp. 838–845. doi: 10.2514/2.4346.

[7] Lee, K.W., and Singh, S.N.," $\mathcal{L}_1$ Adaptive Control of a Nonlinear Aeroelastic System Despite Gust Load, " *Journal of Vibration and Control*, Vol. 19, No. 12, 2013, pp. 1807-1821. doi: 10.1177/1077546312452315.

[8] Gujjula, S, Singh, S.N., and Yim, W., "Adaptive and Neural Control of a Wing Section Using Leading- and Trailing-Edge Surfaces," *Aerospace Science and Technology*, Vol. 9, No. 2, 2005, pp. 161-171. doi: 10.1016/j.ast.2004.10.003.

[9] Ioannou, P.A., and Sun, J., "Robust Adaptive Control", Dover Publications, 2012. Dover, New York. ISBN-10: 0486498174.

[10] Hovakimyan, N. and Cao, C. "L_1 Adaptive Control Theory, Guaranteed Robustness with Fast Adaptation," Vol. 21 of Advances in Design and Control, SIAM, 2010. ISBN-10: 0898717043.

[11] Ko, J., Strganac, T.W., and Kurdila, A.J., "Adaptive Feedback Linearization for the Control of a Typical Wing Section with Structural Nonlinearity," *Nonlinear Dynamics*, Vol. 18, No. 3, 1999, pp. 289–301. doi: 10.1023/A:1008323629064.

[12] Zeng, Y., and Singh, S.N., "Output Feedback Variable Structure Adaptive Control of an Aeroelastic Systems," *Journal of Guidance, Control, and Dynamics*, Vol. 21, No. 6, 1998, pp. 830–837. doi: 10.2514/2.4342.

[13] Xing, W., and Singh, S.N., "Adaptive Output Feedback Control of a Nonlinear Aeroelastic Structure," *Journal of Guidance, Control, and Dynamics*, Vol. 23, No. 6, 2000, pp. 1109–1116. doi: 10.2514/2.4662.

[14] Zhang, R., and Singh, S.N., "Adaptive Output Feedback Control of an Aeroelastic System with Unstructured Uncertainties," *Journal of Guidance, Control, and Dynamics*, Vol. 24, No. 3, 2001, pp. 502–509. doi: 10.2514/2.4739.

[15] Ko, J., and Strganac, T.W., "Stability and Control of a Structurally Nonlinear Aeroelastic System," *Journal of Guidance, Control, and Dynamics*, Vol. 21, No. 5, 1998, pp. 718–725. doi: 10.2514/2.4317.

[16] Fung, Y.C., "An Introduction to the Theory of Aeroelasticity", Dover, New York, 1955. ISBN-10: 0486469360.

[17] Siegfried H. Lehnigk, *On the Hurwitz matrix, Zeitschrift für Angewandte Mathematik und Physik (ZAMP)*, May 1970.

[18] Jafari, S., Ioannou, P.A., Rudd, L., "What is $\mathcal{L}_1$ Adaptive Control", AIAA 2013-4513, *AIAA Guidance, Navigation and Control (GNC) Conference*, August 19-22, 2013, Boston, MA. doi: 10.2514/MGNC13.